# Effects of partial Eu filling in the unfilled skutterudite $CoP_3$

Zicheng Tao [1,*] Chao Zhang [1,*] Jian Yuan,[1] Renjie Zhang,[2,3,4] Xia Wang,[1,5] Zhenhai Yu,[1] Wei Xia,[1,6] Yaobo Huang,[4,7,8] Shihao Zhang,[9,†] and Yanfeng Guo [1,6,‡]

[1]School of Physical Science and Technology, ShanghaiTech University, Shanghai 201210, China
[2]Tsung-Dao Lee Institute, Shanghai Jiao Tong University, Shanghai 200240, China
[3]Beijing National Laboratory for Condensed Matter Physics and Institute of Physics, Chinese Academy of Sciences, Beijing 100190, China
[4]University of Chinese Academy of Sciences, Beijing 100049, China
[5]Analytical Instrumentation Center, School of Physical Science and Technology, ShanghaiTech University, Shanghai 201210, China
[6]ShanghaiTech Laboratory for Topological Physics, Shanghai 201210, China
[7]Shanghai Synchrotron Radiation Facility, Shanghai Advanced Research Institute, Chinese Academy of Sciences, Shanghai 201204, China
[8]Shanghai Institute of Applied Physics, Chinese Academy of Sciences, Shanghai 201800, China
[9]School of Physics and Electronics, Hunan University, Changsha 410082, China

(Received 13 February 2024; revised 22 May 2024; accepted 8 July 2024; published 25 July 2024)

The unfilled skutterudite $CoP_3$ hosts extremely large magnetoresistance ($\sim 2 \times 10^4\%$ at 30 T and 2 K), large hole mobility ($\sim 2 \times 10^4$ cm$^2$ V$^{-1}$ s$^{-1}$, 2 K), and a fourfold quadratic contact point (QCP) above the Fermi level in the electronic structure. We unveil herein that the partial filling of Eu onto the icosahedral void sites of $CoP_3$ can shift the QCP to lie below the Fermi level while retaining the high carrier mobility ($\sim 1.6 \times 10^4$ cm$^2$ V$^{-1}$ s$^{-1}$, 2 K). Unlike nonmagnetic $CoP_3$, partially filled skutterudite $Eu_{0.412}Co_4P_{12}$ is a soft ferromagnet with almost isotropic magnetism. Additionally, an intriguing topological Hall effect is observed, likely hinting an unusual spin texture. In this paper, we provide useful insights into the interplay between magnetism and the nontrivial feature of the electronic band structure, which would guide more efforts in studying this issue.

DOI: 10.1103/PhysRevB.110.035156

## I. INTRODUCTION

The interplay between magnetism and nontrivial topological band structure in magnetic topological phases is one of the research frontiers in topological physics. It can produce fantastic bulk transport properties [1–8] and anomalous surface or edge states [9–21]. Furthermore, the interplay offers an opportunity for magnetic control of different topological phases [22–32]. Unfortunately, the number of natural magnetic topological phases is still very limited, thus hindering the study of this crucial issue as well as the exploration of exotic topological properties. An alternative way to design magnetic topological phases is to dope magnetic elements into nonmagnetic topological phases. An explicit example is the Cr-doped topological insulator (TI) $(Bi, Sb)_2Te_3$ thin film [6], in which the Cr doping breaks the time-reversal symmetry $\mathcal{T}$ and opens a small Dirac mass gap (5–10 meV) in the topological surface state associated with the quantum anomalous Hall (QAH) effect, i.e., the anomalous Hall conductance reaches an $e^2/h$ quantization plateau, through finely tuning the Fermi level ($E_F$) into the surface gap. Since nonmagnetic topological phases usually host rich unique properties, such as various intriguing quasiparticles (Weyl, Dirac, Majorana, nodal line, etc.) [33–42], extremely large magnetoresistance (EXMR) [43], chiral anomaly [44–46], and the quantum spin/anomalous Hall effect [6,47–49], the introduction of magnetism into them offers extraordinary opportunities to study the interplay between magnetism and nontrivial topological states.

In the unfilled skutterudite $CoP_3$, the electronic band structure hosts degenerate bands with a quadratic dispersion along all directions in the momentum space and hence a fourfold quadratic contact point (QCP) at the Γ point of the Brillouin zone (BZ) above $E_F$ of ∼0.146 eV [50]. The QCP phase with a topological number $C = 0$ could be viewed as a parent phase for a variety of topological phases, such as the Weyl semimetal, the $Z_2$ TI/metal, and the Dirac semimetal. Additionally, $CoP_3$ has an EXMR of $\sim 2 \times 10^4\%$ at 30 T and 2 K and very large hole mobility of $\sim 2 \times 10^4$ cm$^2$ V$^{-1}$ s$^{-1}$ at 2 K. These virtues would find potential applications in topological devices. The unit cell of $CoP_3$ consists of eight tilted but corner-connected octahedra formed by P atoms, as shown in Fig. 1(a). The most intriguing aspect of this structure is the presence of two large lattice voids, i.e., the icosahedral voids, with each being surrounded by 12 P atoms. It offers an opportunity to fill these voids by using magnetic elements. It has been demonstrated that filling the voids with small-diameter, large-mass interstitials such as trivalent rare-earth ions in the binary skutterudites $MX_3$ ($M$ = Co, Rh, or Ir; $X$ = P, As, or Sb) can result in low thermal conductivity and hence high thermoelectric efficiency [51]. It has also been unveiled that filled skutterudite compounds with nanostructure display even better thermoelectric performance than conventional bulk material [52].

*The authors contributed equally to this paper.
†Contact author: zhangshh@hnu.edu.cn
‡Contact author: guoyf@shanghaitech.edu.cn

 

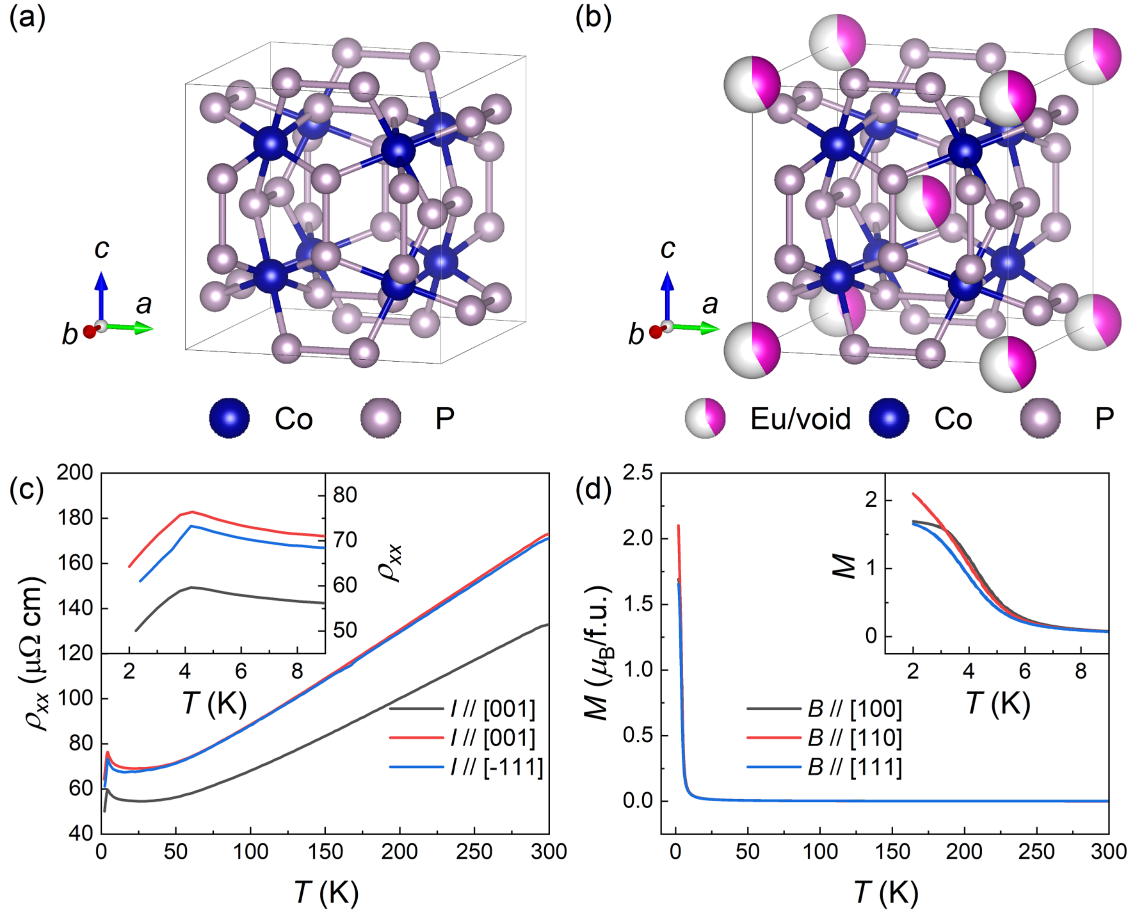


FIG. 1. Views of the schematic crystal structures of (a) $CoP_3$ and (b) $Eu_{0.412}Co_4P_{12}$. (c) Temperature-dependent longitudinal resistivity $\rho_{xx}$ of $Eu_{0.412}Co_4P_{12}$ with the current along the [001], [001], and [−111] directions. (d) Temperature dependence of magnetizations along the [100], [110], and [111] directions at $B = 500$ Oe. The insets of (c) and (d) show the enlarged views of the low-temperature data.

In this paper, we report on the synthesis of single-crystalline $Eu_{0.412}Co_4P_{12}$ with all Eu atoms filling the icosahedral voids of $CoP_3$. In this paper, we unveil that $Eu_{0.412}Co_4P_{12}$ is a soft ferromagnet with $T_C$ of 4.2 K, which retains large carrier mobility and shows intriguing topological Hall effect (THE) near $T_C$. Our first-principles calculations indicate that the QCP is tuned to lie below $E_F$ with slight splitting due to the strong crystalline field of Eu ions.

The details for the morphology of the single crystals, single-crystal x-ray diffraction (SXRD) data, magnetotransport, method of the two-band model fitting, and first-principles calculations of $Eu_{0.412}Co_4P_{12}$ are presented in the Supplemental Material (SM) [53].

## II. EXPERIMENT AND METHODS

Here, $Eu_{0.412}Co_4P_{12}$ single crystals were grown by using the flux method. Starting materials Eu (99.5%, Macklin) blocks, Co (99.99%, Macklin) plates, P (99.999%, aladdin) powder, and Sn (99.99%, Aladdin) granules were mixed in a molar ratio of 1:4:20:50 and placed into an alumina crucible, which was then sealed into a quartz tube in vacuum. The assembly was heated in a furnace up to 1100 °C within 10 h, kept at the temperature for 10 h, and then slowly cooled down to 700 °C at a temperature decreasing rate of 2 °C/h. The excess Sn was removed at this temperature by quickly placing the assembly into a high-speed centrifuge, and black crystals with shining surface in a typical dimension of $2 \times 2 \times 2$ mm$^3$ were obtained. The crystallographic phase and quality examinations of $Eu_{0.412}Co_4P_{12}$ were examined on a Bruker D8 single-crystal x-ray diffractometer with Mo $K\alpha 1$ ($\lambda = 0.71073$ Å) at 278 K, as shown in Figs. S1(a)–1(c) in the SM [53]. The collected SXRD data were analyzed by using the OLEX2 software [54]. The electrical transport measurements, including the resistivity and Hall effect measurements, were carried out by using a standard Hall bar geometry in a commercial DynaCool Physical Properties Measurement System from Quantum Design. The magnetic susceptibility measurements were measured on a Quantum Design Magnetic Properties Measurement System.

The first-principles calculations are carried out within the framework of the generalized gradient approximation functional [55] of the density functional theory in VASP [56]. We employ the Hubbard parameter $U = 5$ eV on the $f$ orbitals of Eu atoms. To study the Eu filling effect, we use the $EuCo_8P_{24}$, $Eu_4Co_{40}P_{120}$, and $Eu_5Co_{48}P_{144}$ supercell model and calculate their energy bands.

TABLE I. Atom occupancy determined for the $Eu_{0.412}Co_4P_{12}$ unit cell.

| Site | Wyckoff | $x$ | $y$ | $z$ | Occupancy | $U_{eq}$ |
|---|---|---|---|---|---|---|
| Eu | $2a$ | 0 | 0 | 0 | 0.412 | 0.007 |
| Co | $8c$ | 0.75 | 0.25 | 0.25 | 1 | 0.004 |
| P | $24g$ | 0.5 | 0.35408 | 0.14861 | 1 | 0.005 |

### III. RESULTS AND DISCUSSION

The crystal structure of the grown crystals is drawn based on the SXRD data refinement, as illustrated in Fig. 1(b). The diffraction patterns could be well indexed based on a cubic unit cell in the space group $Im\bar{3}$ (No. 204) with the lattice parameters $a = b = c = 7.768$ Å and $\alpha = \beta = \gamma = 90°$. Because of the partial filling of Eu onto the void sites, the refined unit cell volume is slightly larger than that of the parent phase $CoP_3$. The occupancy of each atom derived from the refinement is given in Table I, which shows that all Eu atoms are situated at $2a$ (0, 0, 0), and its occupancy is 0.412, nearly approaching the maximal occupancy in the parent lattice, such as the cases of $CoSb_3$ and $FeSb_3$ [57,58].

The temperature-dependent longitudinal resistivity $\rho_{xx}(T)$ of $Eu_{0.412}Co_4P_{12}$ with the electrical current along the [001], [001], and [−111] directions is depicted in Fig. 1(c), which unveils the semimetallic nature of $Eu_{0.412}Co_4P_{12}$ in the temperature range of 2–300 K. The $\rho_{xx}(T)$ curves exhibit a sharp peak at 4.2 K signifying the ferromagnetic (FM) order caused by the filled Eu in $Eu_{0.412}Co_4P_{12}$, which is consistent with the result of magnetization measurements presented in Fig. 1(d). The temperature dependence of magnetization $M(T)$ curves in Fig. 1(d) for $Eu_{0.412}Co_4P_{12}$ under an external magnetic field $B$ of 500 Oe along the crystallographic axes [100], [110], and [111] also expose the FM order.

To elucidate the relationship between the magnetization and magnetotransport properties, the isothermal magnetiza-

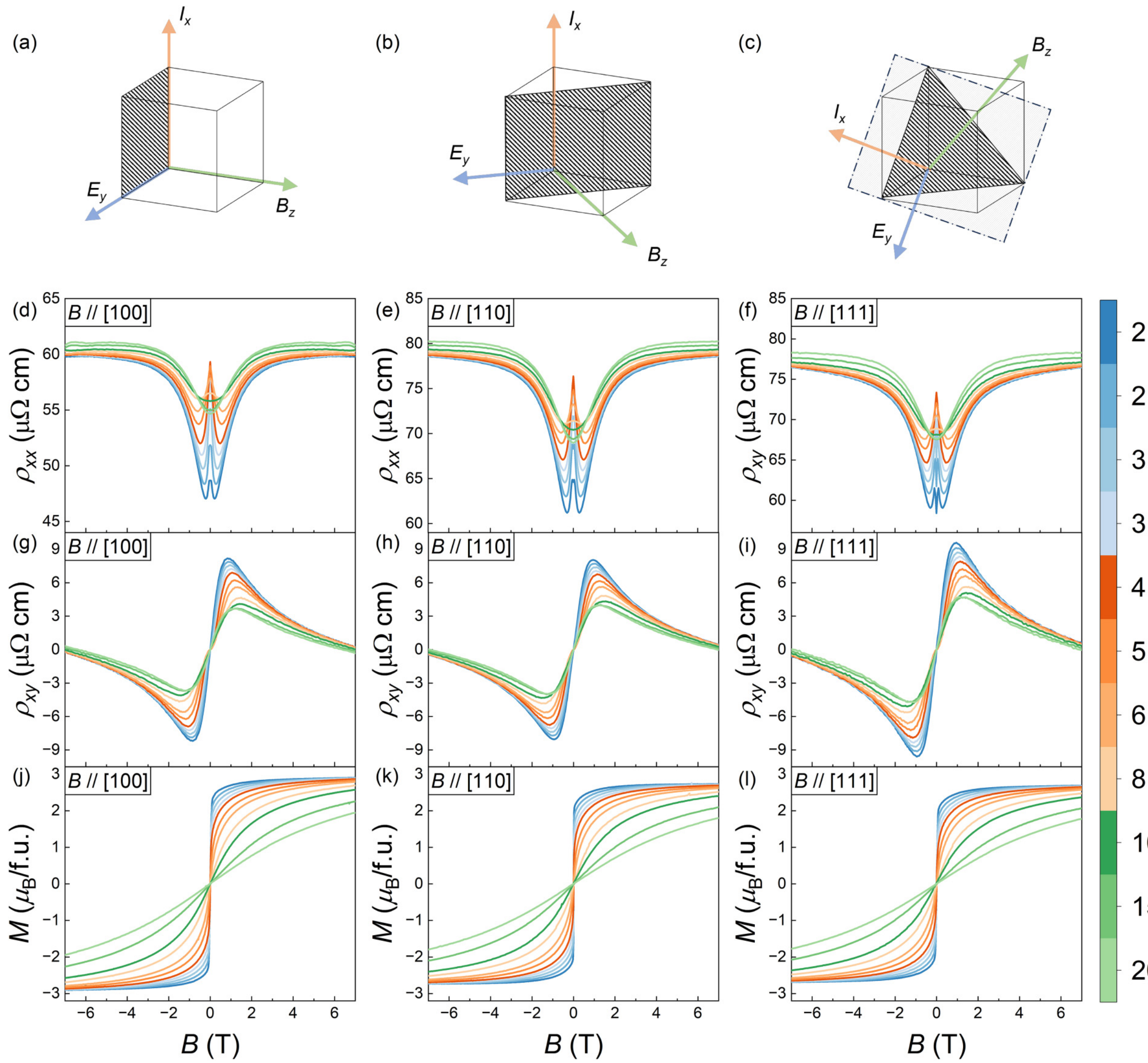


FIG. 2. The measurement configurations for $\rho_{xy}$ of $Eu_{0.412}Co_4P_{12}$ when (a) $B$//[100], (b) $B$//[110], and (c) $B$//[111]. (d)–(l) The field dependence of longitudinal resistivity $\rho_{xx}$, transverse resistivity $\rho_{xy}$, and magnetizations $M$ at various temperatures for $B$ along the [100], [110], and [111] directions, respectively.

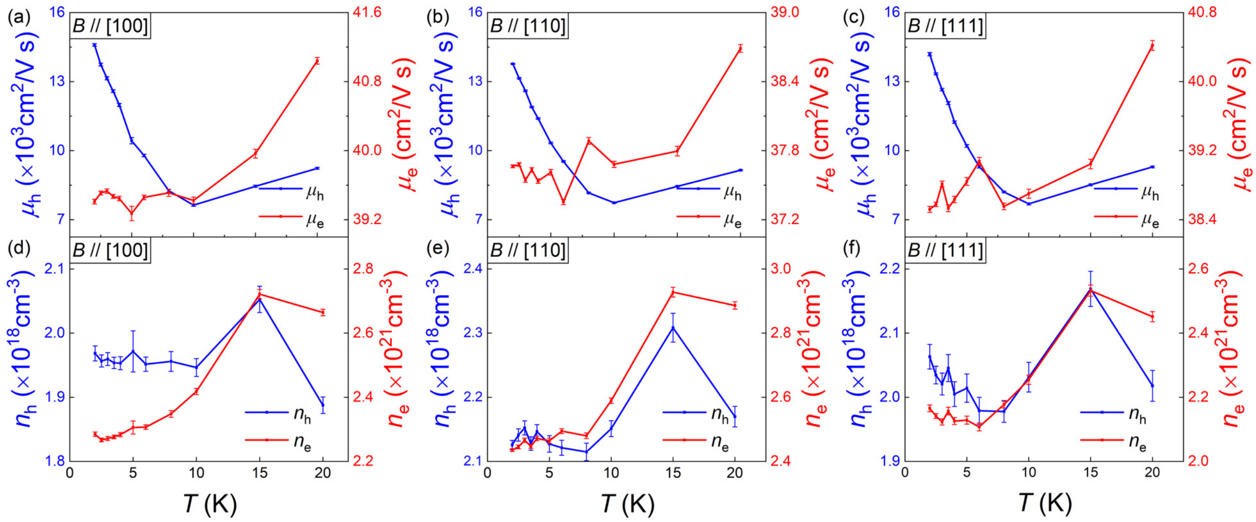


FIG. 3. The hole ($\mu_h$) and electron ($\mu_e$) mobilities at different temperatures for (a) $B$//[100], (b) $B$//[110], and (c) $B$//[111] directions. The hole ($n_h$) and electron ($n_e$) carrier densities at different temperatures for (d) $B$//[100], (e) $B$//[110], and (f) $B$//[111] directions. The error bars are enlarged by a factor of 5.

tion $M(H)$ curves and the corresponding Hall resistivity $\rho_{xy}$ are shown in Fig. 2. The measurement configurations are illustrated in Figs. 2(a)–2(c). The field dependence of $\rho_{xx}$, $\rho_{xy}$, and $M$ for $Eu_{0.412}Co_4P_{12}$ at various temperatures when $B$//[100], [110], and [111] are presented in Figs. 2(d)–2(l), respectively. Apparently, each set of data shows similar behavior, suggesting the weak anisotropy in $Eu_{0.412}Co_4P_{12}$. The $M(H)$ curves clearly demonstrate that $Eu_{0.412}Co_4P_{12}$ is a soft ferromagnet, as shown in Figs. 2(j)–2(l). The saturation magnetic moments at 2 K reach ∼2.90, 2.72, and 2.69 $\mu_B$/f.u. for $B$//[100], [110], and [111] directions, respectively. This is consistent with the fact that divalent Eu (∼7 $\mu_B$/f.u.) is filled with the occupancy number of 0.412. The magnetoresistance (MR), defined as $[\rho(B) - \rho(0)]/\rho(0) \times 100\%$, where $\rho(B)$ and $\rho(0)$ represent the resistivity with and without $B$, respectively, reaches ∼20–30% at 2 K and 7 T for $B$//[100], [110], and [111] directions, as shown in Figs. S3(a)–3(c) in the SM [53], respectively. The values are much smaller than that of $CoP_3$, $\sim3.5 \times 10^3\%$ at 2 K and 9 T. Another clear difference is that the MR of $Eu_{0.412}Co_4P_{12}$ already displays saturation behavior before 7 T, while that of $CoP_3$ nearly shows a quadratic evolution with the magnetic field $B$, i.e., MR $\sim\mu_h\mu_e B^2$ [59,60], without any sign of saturation at 9 T.

To investigate the Hall effect in $Eu_{0.412}Co_4P_{12}$, $\rho_{xy}$ was measured with the magnetic field along [100], [110], and [111] directions at 5 K, as shown in Figs. 3(a)–3(c), respectively. Generally, $\rho_{xy}$ can be expressed as

$$\rho_{xy} = \rho_{xy}^{\mathrm{N}} + \rho_{xy}^{\mathrm{A}} + \rho_{xy}^{\mathrm{T}},$$

where $\rho_{xy}^{\mathrm{N}}$ represents ordinary Hall resistivity; $\rho_{xy}^{\mathrm{A}}$ $(= R_{\mathrm{S}}4\pi M)$ is anomalous Hall resistivity, with $R_{\mathrm{S}}$ denoting the anomalous Hall coefficient; and $\rho_{xy}^{\mathrm{T}}$ represents the topological Hall resistivity [61,62]. To quantitatively estimate the densities and mobilities of the carriers, $\rho_{xy}^{\mathrm{N}}$ was fitted by employing the conventional two-band model [63]:

$$\rho_{xy}^{\mathrm{N}} = \frac{\left(n_h\mu_h^2 - n_e\mu_e^2\right) + \mu_h^2\mu_e^2(n_h - n_e)B^2}{(n_e\mu_e + n_h\mu_h)^2 + \mu_h^2\mu_e^2(n_h - n_e)^2B^2}\frac{B}{e},$$

where $n_e$ ($n_h$) denotes the carrier density for the electron (hole), and $\mu_e$ ($\mu_h$) is the mobility of the electron (hole). The fitting at 2 K yields $\mu_h$ of $1.46 \times 10^4$ cm$^2$ V$^{-1}$ s$^{-1}$ and $\mu_e$ of 39.4 cm$^2$ V$^{-1}$ s$^{-1}$ when $B$//[100], unveiling high hole mobilities close to that of the parent phase $CoP_3$ and largely reduced electron mobilities. It unambiguously indicates the variation of the electronic band structure around $E_{\mathrm{F}}$. The corresponding carrier densities are $1.97 \times 10^{18}$ and $2.28 \times 10^{21}$ cm$^{-3}$ for holes and electrons, respectively. The fitting results at different temperatures along the three directions are summarized in Figs. 3(a)–3(f). The hole mobilities are approximately three orders of magnitude larger than that of the electrons below 20 K, while the carrier densities for holes are approximately three orders of magnitude smaller than that of electrons. For $B$ along different directions, the mobilities and carrier densities of holes (electrons) each are at the same magnitude, which exhibit similar evolution trends with temperature, indicating weak anisotropy in the electronic band structure of $Eu_{0.412}Co_4P_{12}$.

It is obvious that $R_{\mathrm{S}} \sim 0$ in $Eu_{0.412}Co_4P_{12}$, as discussed in the SM [53]. The topological Hall resistivity $\rho_{xy}^{\mathrm{T}}$ is derived by subtracting $\rho_{xy}^{\mathrm{N}}$ from $\rho_{xy}$, which is presented in Figs. 4(d)–4(f) below 20 K for the [100], [110], and [111] directions, respectively. It is apparent that the THE is more pronounced at 5 K for all three directions. In addition, the $\rho_{xy}^{\mathrm{T}}$ curves along three different directions are nearly copied one by one with the peak values being very close; those are 1.8 $\mu\Omega$ cm for $B$//[100] at $B = 0.35$ T, 1.6 $\mu\Omega$ cm for $B$//[110] at $B = 0.33$ T, and 1.8 $\mu\Omega$ cm for $B$//[111] at $B = 0.35$ T. In this case, $Eu_{0.412}Co_4P_{12}$ is centrosymmetric and magnetically isotropic, which excludes the helical topological magnetic structures, i.e., the magnetic skyrmions, as the source for the THE because such a unique magnetic structure is usually stabilized in noncentrosymmetric structures with Dzyaloshinskii-Moriya interaction or, alternatively, by the competition between magnetic dipole interaction and strong perpendicular uniaxial anisotropy. Other possibilities, including the domain wall skew scattering which is irrelevant to spin chirality [64,65], etc., should be carefully examined in the future.

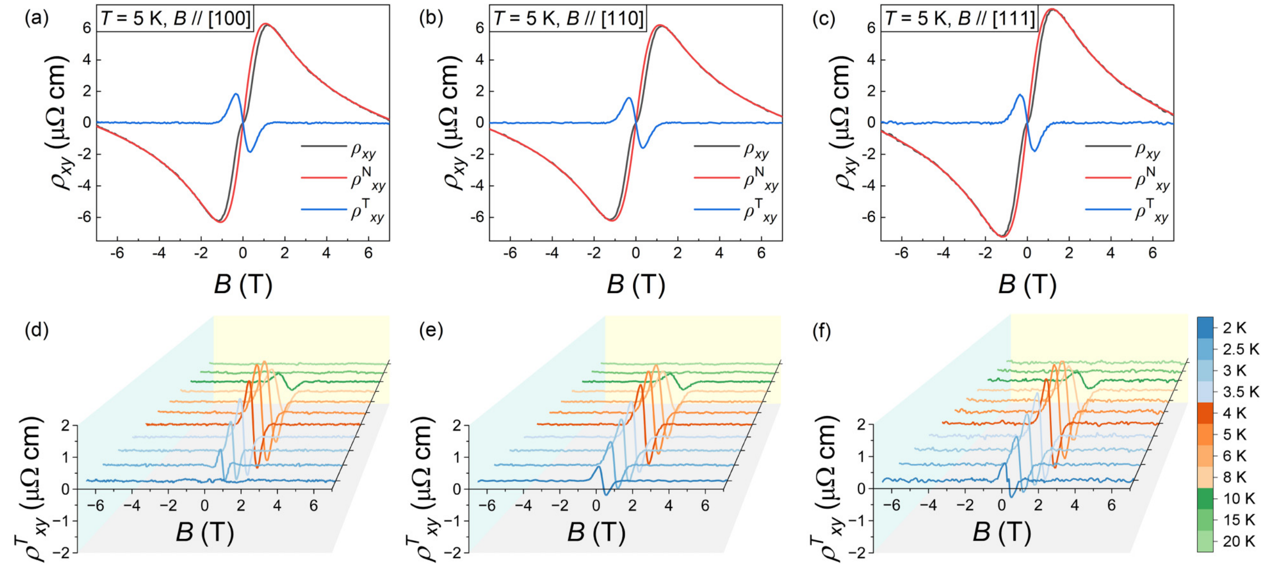


FIG. 4. (a)–(c) Hall resistivity $\rho_{xy}$, fitted ordinary Hall resistivity $\rho_{xy}^{\mathrm{N}}$, and topological Hall resistivity $\rho_{xy}^{\mathrm{T}}$ after subtracting other signals at a temperature of 5 K for $B$//[100], [110], and [111], respectively. (d)–(f) Topological Hall resistivity $\rho_{xy}^{\mathrm{T}}$ vs $B$ at various temperatures for $B$//[100], [110], and [111], respectively.

To study the Eu filling effect on the electronic band structure of $CoP_3$, first-principles calculations on $Eu_{0.412}Co_4P_{12}$ are carried out. The results reveal that the magnetic anisotropy of $Eu_{0.412}Co_4P_{12}$ is only 2 $\mu$eV per Eu atom, implying that its spin direction can be easily tuned by applying an external magnetic field. As shown in Figs. 5(a)–5(b), compared with bulk $CoP_3$ in which the QCP is above $E_F$, the QCP of $Eu_{0.412}Co_4P_{12}$ is tuned to lie below $E_F$ due to electron transfer between P and Eu atoms and the enhanced crystalline field of Co ions. It is crucial because, in such a case, the QCP could dominate the low-energy electronic structure. The electronic states near the QCP in three Eu filling cases are also calculated and presented in Figs. 5(e)–5(h). In the pristine bulk $CoP_3$ with $T_h$ point symmetry, the energy bands near the QCP belong to $\Gamma_2^-$ and $\Gamma_3^-$ irreducible representations, which have different eigenvalues of $C_3$ operation and hold the symmetry-protected QCP, as shown in Fig. 5(e). When Eu is filled, it is noted that the QCP is somewhat broken by the

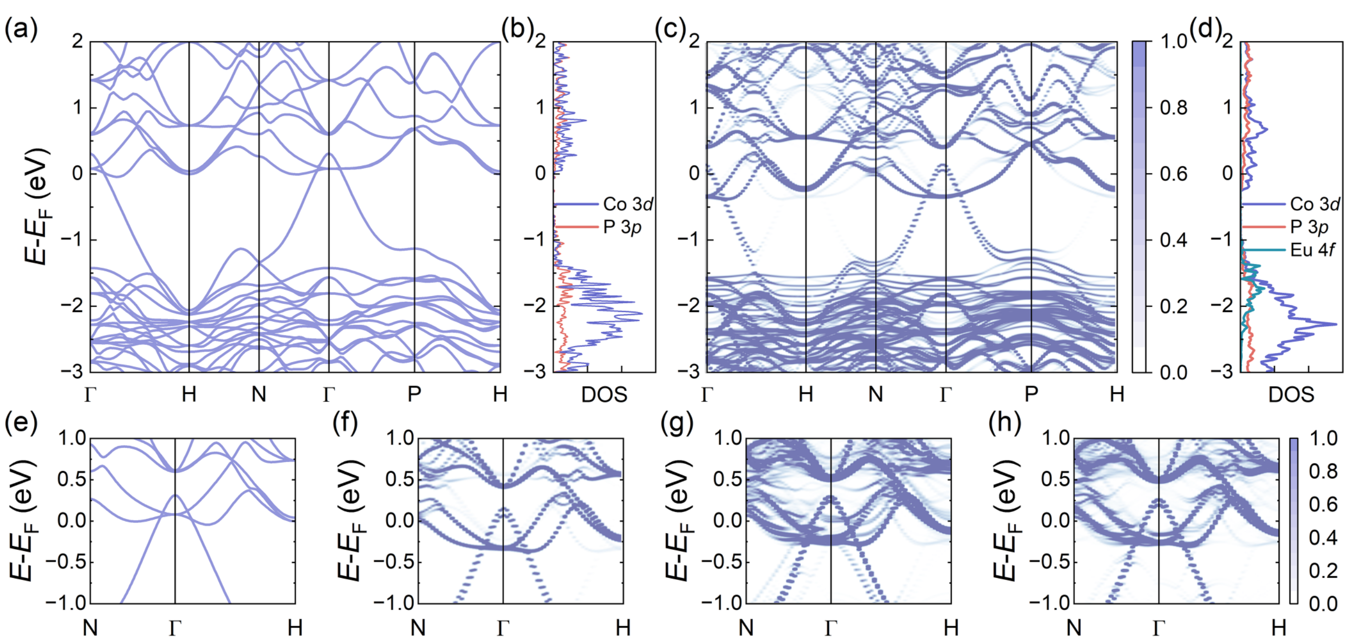


FIG. 5. (a) The energy bands of bulk $CoP_3$. The projected density of states (DOS) contributed by $d$ orbitals of Co and $p$ orbitals of P are present in (b). The unfolded energy bands of $Eu_{0.5}Co_4P_{12}$ are shown in (c), and projected DOS are present in (d). The on-site Hubbard interaction is chosen as $U = 5$ eV on the $f$ orbitals of Eu atoms. The Eu-$f$ orbitals are mainly located ∼1.8 eV below $E_F$. The electronic states near the quadratic contact point (QCP) of bulk $CoP_3$ are present in (e). Three possible Eu filling cases are also shown as (f) $Eu_{0.5}Co_4P_{12}$, (g) $Eu_{0.4}Co_4P_{12}$, and (h) $Eu_{0.416}Co_4P_{12}$.

crystalline field of Eu ions, as shown in Figs. 5(f)–5(h), but the dispersionless cones contributed by $p$ orbitals of P near $E_F$ are negligibly influenced by the crystalline field of Eu ions. Thus, it still holds the carriers with small effective electron masses and high mobilities like those of bulk $CoP_3$.

Our magnetization measurements indicate divalent Eu ions in $Eu_{0.412}Co_4P_{12}$. Usually, the crystalline field effect in $Eu^{2+}$ compounds can be ignored due to the $4f^7$ electronic configuration of $Eu^{2+}$ ions with an orbital angular momentum $L = 0$. However, as shown in Figs. 5(e)–5(f), the energy bands contributed by the $d$ orbitals of Co atoms shift downward, indicating that Eu doping induces the electron transfer between the Eu atom and neighboring P atoms. Thus, the P atoms with more electrons lead to the enhanced crystalline field near the Co atoms. Furthermore, comparing Fig. 5(a) and Fig. S5 in the SM [53], the influence of the lattice expansion and displacement of Co atoms on the dispersion of the energy bands contributed by the $d$ orbitals of Co atoms near the Fermi level could be excluded. Considering the more complex situation in $Eu_{0.412}Co_4P_{12}$, Eu ions occupy specific positions in the lattice, and Co atoms are influenced by the inhomogeneous electrostatic field of the surrounding coordinating atoms, forming a low-symmetry crystalline field. This crystalline field breaks the nontrivial topological electronic band structure, i.e., the QCP in $Eu_{0.412}Co_4P_{12}$, which could explain the largely reduced MR as compared with $CoP_3$. Conversely, the dispersionless band cones contributed by $p$ orbitals of P atoms near $E_F$ are negligibly influenced by the crystalline field. Thus, it still holds the characteristics of carriers with small effective electron masses and high mobilities, which are like those of bulk $CoP_3$. The THE observed in $Eu_{0.412}Co_4P_{12}$ is difficult to be explained through large-scale first-principles calculations. This observation suggests a promising avenue for future investigations on the magnetic structure. Further experimental and theoretical studies are necessary not only to elucidate the origin of the THE in $Eu_{0.412}Co_4P_{12}$ but also to gain a deep understanding about the interplay between the magnetic structure and the nontrivial topological electronic band structure in $Eu_{0.412}Co_4P_{12}$.

## IV. SUMMARY

To summarize, the partially filled skutterudite $Eu_{0.412}Co_4P_{12}$ is a soft ferromagnet with $T_C$ of 4.2 K and weak magnetic anisotropy. The Eu filling shifts the QCP to lie below the Fermi level, which is crucial to dominate the low-energy electronic properties. The QCP is somewhat broken due to the inhomogeneous crystalline field induced by Eu ions, while the dispersionless band cones formed by the $p$ orbitals of P near the Fermi level are negligibly affected, which is the reason that high carrier mobilities and small effective mass are still retained. Moreover, $Eu_{0.412}Co_4P_{12}$ also exhibits THE, which provides an opportunity to study the intriguing magnetic structure. In this paper, we offer useful insights into the coupling between magnetism and electronic band structure in topological materials.

## ACKNOWLEDGMENTS

The authors acknowledge the support by the National Natural Science Foundation of China (Grants No. 92065201 and No. 12304217) and the National Key R&D Program of China (Grant No. 2023YFA1406100). Y.F.G. acknowledges the open projects from State Key Laboratory of Functional Materials for Informatics (Grant No. SKL2022), CAS, and Beijing National Laboratory for Condensed Matter Physics (Grant No. 2023BNLCMPKF002). Part of this paper is supported by the RIXS endstation at BL09UC in the Shanghai Synchrotron Radiation Facility. Y.B.H. acknowledges the Shanghai Municipal Science and Technology Major Project. The authors also thank the Analytical Instrumentation Center (Grant No. SPST-AIC10112914) and the Double First-Class Initiative Fund of ShanghaiTech University for support. S.H.Z. acknowledges the Fundamental Research Funds for the Central Universities from China.

[1] Q. Wang, Y. Xu, R. Lou, Z. Liu, M. Li, Y. Huang, D. Shen, H. Weng, S. Wang, and H. Lei, Large intrinsic anomalous Hall effect in half-metallic ferromagnet $Co_3Sn_2S_2$ with magnetic Weyl fermions, Nat. Commun. **9**, 3681 (2018).

[2] M. Ikhlas, T. Tomita, T. Koretsune, M.-T. Suzuki, D. Nishio-Hamane, R. Arita, Y. Otani, and S. Nakatsuji, Large anomalous Nernst effect at room temperature in a chiral antiferromagnet, Nat. Phys. **13**, 1085 (2017).

[3] S. Nakatsuji, N. Kiyohara, and T. Higo, Large anomalous Hall effect in a non-collinear antiferromagnet at room temperature, Nature (London) **527**, 212 (2015).

[4] E. J. Cheng, W. Xia, X. B. Shi, H. W. Fang, C. W. Wang, C. Y. Xi, S. W. Xu, D. C. Peets, L. S. Wang, H. Su *et al.*, Magnetism-induced topological transition in $EuAs_3$, Nat. Commun. **12**, 6970 (2021).

[5] A. K. Nayak, J. E. Fischer, Y. Sun, B. Yan, J. Karel, A. C. Komarek, C. Shekhar, N. Kumar, W. Schnelle, J. Kubler *et al.*, Large anomalous Hall effect driven by a nonvanishing Berry curvature in the noncolinear antiferromagnet $Mn_3Ge$, Sci. Adv. **2**, e1501870 (2016).

[6] C.-Z. Chang, J. Zhang, X. Feng, J. Shen, Z. Zhang, M. Guo, K. Li, Y. Ou, P. Wei, L.-L. Wang *et al.*, Experimental observation of the quantum anomalous Hall effect in a magnetic topological insulator, Science **340**, 167 (2013).

[7] M. Mogi, M. Kawamura, A. Tsukazaki, R. Yoshimi, K. S. Takahashi, M. Kawasaki, and Y. Tokura, Tailoring tricolor structure of magnetic topological insulator for robust axion insulator, Sci. Adv. **3**, eaao1669 (2017).

[8] D. Xiao, J. Jiang, J. H. Shin, W. Wang, F. Wang, Y.-F. Zhao, C. Liu, W. Wu, M. H. W. Chan, N. Samarth *et al.*, Realization of the axion insulator state in quantum anomalous Hall sandwich heterostructures, Phys. Rev. Lett. **120**, 056801 (2018).

[9] L. Ye, M. Kang, J. Liu, F. von Cube, C. R. Wicker, T. Suzuki, C. Jozwiak, A. Bostwick, E. Rotenberg, D. C. Bell *et al.*, Massive Dirac fermions in a ferromagnetic kagome metal, Nature (London) **555**, 638 (2018).

[10] N. Morali, R. Batabyal, P. K. Nag, E. Liu, Q. Xu, Y. Sun, B. Yan, C. Felser, N. Avraham, and H. Beidenkopf, Fermi-arc diversity on surface terminations of the magnetic Weyl semimetal $Co_3Sn_2S_2$, Science **365**, 1286 (2019).

[11] L. Xu, Y. Mao, H. Wang, J. Li, Y. Chen, Y. Xia, Y. Li, D. Pei, J. Zhang, H. Zheng *et al.*, Persistent surface states with diminishing gap in $MnBi_2Te_4/Bi_2Te_3$ superlattice antiferromagnetic topological insulator, Sci. Bull. **65**, 2086 (2020).
[12] Y.-J. Hao, P. Liu, Y. Feng, X.-M. Ma, E. F. Schwier, M. Arita, S. Kumar, C. W. Hu, R. Lu, M. Zeng *et al.*, Gapless surface Dirac cone in antiferromagnetic topological insulator $MnBi_2Te_4$, Phys. Rev. X **9**, 041038 (2019).
[13] X. Wu, J. Li, X.-M. Ma, Y. Zhang, Y. Liu, C.-S. Zhou, J. Shao, Q. Wang, Y.-J. Hao, Y. Feng *et al.*, Distinct topological surface states on the two terminations of $MnBi_4Te_7$, Phys. Rev. X **10**, 031013 (2020).
[14] R. C. Vidal, A. Zeugner, J. I. Facio, R. Ray, M. H. Haghighi, A. U. B. Wolter, L. T. C. Bohorquez, F. Caglieris, S. Moser, T. Figgemeier *et al.*, Topological electronic structure and intrinsic magnetization in $MnBi_4Te_7$: A $Bi_2Te_3$ derivative with a periodic Mn sublattice, Phys. Rev. X **9**, 041065 (2019).
[15] Y. J. Chen, L. X. Xu, J. H. Li, Y. W. Li, H. Y. Wang, C. F. Zhang, H. Li, Y. Wu, A. J. Liang, C. Chen *et al.*, Topological electronic structure and its temperature evolution in antiferromagnetic topological insulator $MnBi_2Te_4$, Phys. Rev. X **9**, 041040 (2019).
[16] D. Nevola, H. X. Li, J.-Q. Yan, R. G. Moore, H.-N. Lee, H. Miao, and P. D. Johnson, Coexistence of surface ferromagnetism and a gapless topological state in $MnBi_2Te_4$, Phys. Rev. Lett. **125**, 117205 (2020).
[17] Y. Gong, J. Guo, J. Li, K. Zhu, M. Liao, X. Liu, Q. Zhang, L. Gu, L. Tang, X. Feng *et al.*, Experimental realization of an intrinsic magnetic topological insulator, Chin. Phys. Lett. **36**, 076801 (2019).
[18] H. Li, S.-Y. Gao, S.-F. Duan, Y.-F. Xu, K.-J. Zhu, S.-J. Tian, J.-C. Gao, W.-H. Fan, Z.-C. Rao, J.-R. Huang *et al.*, Dirac surface states in intrinsic magnetic topological insulators $EuSn_2As_2$ and $MnBi_{2n}Te_{3n+1}$, Phys. Rev. X **9**, 041039 (2019).
[19] M. M. Otrokov, I. I. Klimovskikh, H. Bentmann, D. Estyunin, A. Zeugner, Z. S. Aliev, S. Gaß, A. U. B. Wolter, A. V. Koroleva, A. M. Shikin *et al.*, Prediction and observation of an antiferromagnetic topological insulator, Nature (London) **576**, 416 (2019).
[20] E. D. L. Rienks, S. Wimmer, J. Sánchez-Barriga, O. Caha, P. S. Mandal, J. Růžička, A. Ney, H. Steiner, V. V. Volobuev, H. Groiss *et al.*, Large magnetic gap at the Dirac point in $Bi_2Te_3/MnBi_2Te_4$ heterostructures, Nature (London) **576**, 423 (2019).
[21] K. N. Gordon, H. Sun, C. Hu, A. G. Linn, H. Li, Y. Liu, P. Liu, S. Mackey, Q. Liu, N. Ni *et al.*, Strongly gapped topological surface states on protected surfaces of antiferromagnetic $MnBi_4Te_7$ and $MnBi_6Te_{10}$, arXiv:1910.13943.
[22] C. Liu, Y. Wang, H. Li, Y. Wu, Y. Li, J. Li, K. He, Y. Xu, J. Zhang, and Y. Wang, Robust axion insulator and Chern insulator phases in a two-dimensional antiferromagnetic topological insulator, Nat. Mater. **19**, 522 (2020).
[23] D. Zhang, M. Shi, T. Zhu, D. Xing, H. Zhang, and J. Wang, Topological axion states in the magnetic insulator $MnBi_2Te_4$ with the quantized magnetoelectric effect, Phys. Rev. Lett. **122**, 206401 (2019).
[24] C. Hu, L. Ding, K. N. Gordon, B. Ghosh, H.-J. Tien, H. Li, A. G. Linn, S. W. Lien, C.-Y. Huang, S. Mackey *et al.*, Realization of an intrinsic ferromagnetic topological state in $MnBi_8Te_{13}$, Sci. Adv. **6**, eaba4275 (2020).
[25] M. M. Otrokov, I. P. Rusinov, M. Blanco-Rey, M. Hoffmann, A. Y. Vyazovskaya, S. V. Eremeev, A. Ernst, P. M. Echenique, A. Arnau, and E. V. Chulkov, Unique thickness-dependent properties of the van der Waals interlayer antiferromagnet $MnBi_2Te_4$ films, Phys. Rev. Lett. **122**, 107202 (2019).
[26] H. Su, B. C. Gong, W. J. Shi, H. F. Yang, H. Y. Wang, W. Xia, Z. H. Yu, P. J. Guo, J. H. Wang, L. C. Ding *et al.*, Magnetic exchange induced Weyl state in a semimetal $EuCd_2Sb_2$, APL Mater. **8**, 011109 (2020).
[27] S. C. Huan, D. H. Wang, H. Su, H. Y. Wang, X. Wang, N. Yu, Z. Q. Zou, H. J. Zhang, and Y. F. Guo, Magnetism induced ideal Weyl state in bulk van der Waals crystal $MnSb_2Te_4$, Appl. Phys. Lett. **118**, 192105 (2021).
[28] S. C. Huan, S. H. Zhang, Z. C. Jiang, H. Su, H. Y. Wang, X. Zhang, Y. C. Yang, Z. T. Liu, X. Wang, N. Yu *et al.*, Multiple magnetic topological phases in bulk van der Waals crystal $MnSb_4Te_7$, Phys. Rev. Lett. **126**, 246601 (2021).
[29] W. L. Liu, X. Zhang, S. M. Nie, Z. T. Liu, X. Y. Sun, H. Y. Wang, J. Y. Ding, L. Sun, Z. Huang, H. Su *et al.*, Spontaneous ferromagnetism induced topological phase transition in $EuB_6$, Phys. Rev. Lett. **129**, 166402 (2022).
[30] J. Yuan, X. B. Shi, H. Su, X. Zhang, X. Wang, N. Yu, Z. Q. Zou, W. W. Zhao, J. P. Liu, and Y. F. Guo, Magnetization tunable Weyl states in $EuB_6$, Phys. Rev. B **106**, 054411 (2022).
[31] T. Suzuki, L. Savary, J.-P. Liu, J. W. Lynn, L. Balents, and J. G. Checkelsky, Singular angular magnetoresistance in a magnetic nodal semimetal, Science **365**, 377 (2019).
[32] J. Liu and L. Balents, Anomalous Hall effect and topological defects in antiferromagnetic Weyl semimetals: $Mn_3Sn/Ge$, Phys. Rev. Lett. **119**, 087202 (2017).
[33] S. M. Young, S. Zaheer, J. C. Y. Teo, C. L. Kane, E. J. Mele, and A. M. Rappe, Dirac semimetal in three dimensions, Phys. Rev. Lett. **108**, 140405 (2012).
[34] Z. Wang, H. Weng, Q. Wu, X. Dai, and Z. Fang, Three-dimensional Dirac semimetal and quantum transport in $Cd_3As_2$, Phys. Rev. B **88**, 125427 (2013).
[35] Z. K. Liu, J. Jiang, B. Zhou, Z. J. Wang, Y. Zhang, H. M. Weng, D. Prabhakaran, S.-K. Mo, H. Peng, P. Dudin *et al.*, A stable three-dimensional topological Dirac semimetal $Cd_3As_2$, Nat. Mater. **13**, 677 (2014).
[36] Z. K. Liu, B. Zhou, Y. Zhang, Z. J. Wang, H. M. Weng, D. Prabhakaran, S.-K. Mo, Z. X. Shen, Z. Fang, X. Dai *et al.*, Discovery of a three-dimensional topological Dirac semimetal, $Na_3Bi$, Science **343**, 864 (2014).
[37] B. Q. Lv, H. M. Weng, B. B. Fu, X. P. Wang, H. Miao, J. Ma, P. Richard, X. C. Huang, L. X. Zhao, G. F. Chen *et al.*, Experimental discovery of Weyl semimetal TaAs, Phys. Rev. X **5**, 031013 (2015).
[38] S.-Y. Xu, I. Belopolski, N. Alidoust, M. Neupane, G. Bian, C. L. Zhang, R. Sankar, G. Q. Chang, Z. J. Yuan, C.-C. Lee *et al.*, Discovery of a Weyl fermion semimetal and topological Fermi arcs, Science **349**, 613 (2015).
[39] G. Chang, S.-Y. Xu, B. J. Wieder, D. S. Sanchez, S.-M. Huang, I. Belopolski, T.-R. Chang, S. Zhang, A. Bansil, H. Lin *et al.*, Unconventional chiral fermions and large topological fermi arcs in RhSi, Phys. Rev. Lett. **119**, 206401 (2017).
[40] H. Weng, C. Fang, Z. Fang, B. A. Bernevig, and X. Dai, Weyl semimetal phase in noncentrosymmetric transition-metal monophosphides, Phys. Rev. X **5**, 011029 (2015).

[41] L. Fu and C. L. Kane, Superconducting proximity effect and Majorana fermions at the surface of a topological insulator, Phys. Rev. Lett. **100**, 096407 (2008).

[42] E. Tang and L. Fu, Strain-induced partially flat band, helical snake states and interface superconductivity in topological crystalline insulators, Nat. Phys. **10**, 964 (2014).

[43] T. Liang, Q. Gibson, M. N. Ali, M. H. Liu, R. J. Cava, and N. P. Ong, Ultrahigh mobility and giant magnetoresistance in the Dirac semimetal $Cd_3As_2$, Nat. Mater. **14**, 280 (2015).

[44] A. A. Zyuzin and A. A. Burkov, Topological response in Weyl semimetals and the chiral anomaly, Phys. Rev. B **86**, 115133 (2012).

[45] J. Xiong, S. K. Kushwaha, T. Liang, J. W. Krizan, M. Hirschberger, W. Wang, R. J. Cava, and N. P. Ong, Evidence for the chiral anomaly in the Dirac semimetal $Na_3Bi$, Science **350**, 413 (2015).

[46] X. Huang, L. Zhao, Y. Long, P. Wang, D. Chen, Z. Yang, H. Liang, M. Xue, H. Weng, Z. Fang *et al.*, Observation of the chiral-anomaly-induced negative magnetoresistance in 3D Weyl semimetal TaAs, Phys. Rev. X **5**, 031023 (2015).

[47] A. T. Lonchakov, S. B. Bobin, V. V. Deryushkin, and V. N. Neverov, Observation of quantum topological Hall effect in the Weyl semimetal candidate HgSe, J. Phys.: Cond. Matter. **31**, 405706 (2019).

[48] H. M. Weng, R. Yu, X. Hu, X. Dai, and Z. Fang, Quantum anomalous Hall effect and related topological electronic states, Adv. Phys. **64**, 227 (2015).

[49] A. A. Burkov, Anomalous Hall effect in Weyl metals, Phys. Rev. Lett. **113**, 187202 (2014).

[50] C. X. Fan, J. Yuan, X. B. Shi, Y. C. Yang, C. Y. Xi, L. Pi, X. Wang, N. Yu, Z. Q. Zou, B. T. Wang *et al.*, Extremely large magnetoresistance in an unfilled skutterudite quadratic contact point semimetal $CoP_3$, Appl. Phys. Lett. **122**, 253103 (2023).

[51] G. S. Nolas, M. Kaeser, R. T. Littleton, and T. M. Tritt IV, High figure of merit in partially filled ytterbium skutterudite materials, Appl. Phys. Lett. **77**, 1855 (2000).

[52] P. C. Zhai, W. Y. Zhao, Y. Li, L. S. Liu, X. F. Tang, Q. J. Zhang, and M. Niino, Nanostructures and enhanced thermoelectric properties in Ce-filled skutterudite bulk materials, Appl. Phys. Lett. **89**, 052111 (2006).

[53] See Supplemental Material at http://link.aps.org/supplemental/10.1103/PhysRevB.110.035156 for the details of the morphology of the single crystals, SXRD data, magnetotransport, method of the two-band model fitting, and first-principles calculations of $Eu_{0.412}Co_4P_{12}$.

[54] O. V. Dolomanov, L. J. Bourhis, R. J. Gildea, J. A. K. Howard, and H. Puschmann, *OLEX2*: A complete structure solution, refinement and analysis program, J. Appl. Cryst. **42**, 339 (2009).

[55] J. P. Perdew, K. Burke, and M. Ernzerhof, Generalized gradient approximation made simple, Phys. Rev. Lett. **77**, 3865 (1996).

[56] G. Kresse and J. Hafner, *Ab initio* molecular dynamics for liquid metals, Phys. Rev. B **47**, 558 (1993).

[57] J. Y. Peng, J. Y. Yang, X. L. Song, Y. H. Chen, and T. J. Zhang, Effect of Fe substitution on the thermoelectric transport properties of $CoSb_3$-based skutterudite compound, J. Alloy. Compd. **426**, 7 (2006).

[58] A. Grytsiv, P. Rogl, S. Berger, C. Paul, E. Bauer, C. Godart, B. Ni, M. M. Abd-Elmeguid, A. Saccone, R. Ferro *et al.*, Structure and physical properties of the thermoelectric skutterudites $Eu_yFe_{4-x}Co_xSb_{12}$, Phys. Rev. B **66**, 094411 (2002).

[59] G. Q. Chang, S. Y. Xu, H. Zheng, C. C. Lee, S. M. Huang, I. Belopolski, D. S. Sanchez, G. Bian, N. Alidoust, T. R. Chang *et al.*, Signatures of fermi arcs in the quasiparticle interferences of the Weyl semimetals TaAs and NbP, Phys. Rev. Lett. **116**, 066601 (2016).

[60] F. Arnold, M. Naumann, S. C. Wu, Y. Sun, M. Schmidt, H. Borrmann, C. Felser, B. Yan, and E. Hassinger, Chiral Weyl pockets and Fermi surface topology of the Weyl semimetal TaAs, Phys. Rev. Lett. **117**, 146401 (2016).

[61] A. Neubauer, C. Pfleiderer, B. Binz, A. Rosch, R. Ritz, P. G. Niklowitz, and P. Boni, Topological Hall effect in the $\mathcal{A}$ phase of MnSi, Phys. Rev. Lett. **102**, 186602 (2009).

[62] N. Kanazawa, Y. Onose, T. Arima, D. Okuyama, K. Ohoyama, S. Wakimoto, K. Kakurai, S. Ishiwata, and Y. Tokura, Large topological Hall effect in a short-period helimagnet MnGe, Phys. Rev. Lett. **106**, 156603 (2011).

[63] L. Zhao, Q. Xu, X. Wang, J. He, J. Li, H. Yang, Y. Long, D. Chen, H. Liang, C. Li *et al.*, Magnetotransport properties in a compensated semimetal gray arsenic, Phys. Rev. B **95**, 115119 (2017).

[64] S. Sorn and A. Paramekanti, Domain wall skew scattering in ferromagnetic Weyl metals, Phys. Rev. B **103**, 104413 (2021).

[65] W. Xia, B. Bai, X. J. Chen, Y. C. Yang, Y. Zhang, J. Yuan, Q. Li, K. Y. Yang, X. Q. Liu, Y. Shi *et al.*, Giant domain wall anomalous Hall effect in an antiferromagnet, arXiv:2312.07336.